PHILOSOPHICAL TRANSACTIONS A

royalsocietypublishing.org/journal/rsta

Research

Cite this article: Holschuh N, Eisen O, Carter C, Franke S, Helm V, Hoffman AO, Paden J, Christianson K. 2026 Radar swath imaging of glaciers and ice sheets. *Phil. Trans. R. Soc. A* **384**: 20240549.
https://doi.org/10.1098/rsta.2024.0549

Received: 6 August 2025
Accepted: 16 January 2026

One contribution of 16 to a Theo Murphy meeting issue 'Next generation ice-sheet bed measurements'.

Subject Areas:
glaciology, geophysics

Keywords:
radioglaciology, Antarctica, geophysics

Author for correspondence:
Nicholas Holschuh
e-mail: nholschuh@amherst.edu

Radar swath imaging of glaciers and ice sheets

Nicholas Holschuh[1], Olaf Eisen[2], Charlotte Carter[3], Steven Franke[4], Veit Helm[3], Andrew O. Hoffman[5,6], John Paden[7] and Knut Christianson[8]

[1]Department of Geology, Amherst College, Amherst, MA, USA
[2]Universität Bremen, Bremen, Germany
[3]Alfred Wegener Institute for Marine and Polar Research, Bremerhaven, Hofbräu München, Germany
[4]Universitatsklinikum Tubingen, Tübingen, Baden-Württemberg, Germany
[5]Columbia University Lamont-Doherty Earth Observatory, Palisades, NY, USA
[6]Department of Earth, Environmental and Planetary Sciences, Rice University, Houston, TX 77005, USA
[7]Center for Remote Sensing of Ice Sheets, Lawrence, KS, USA
[8]University of Washington, Seattle, WA, USA

NH, 0000-0003-1703-5085; OE, 0000-0002-6380-962X

Multichannel ice-penetrating radar systems can be used to generate radar volumes: three-dimensional data structures that capture variability in backscattering intensity as a function of along-track position, two-way travel time and elevation angle. By digitizing surfaces within these data volumes, the production of wide-area, fine-resolution digital elevation models (DEMs) of the ice-bottom interface (measured through kilometres of ice) is now possible. This paper reviews this technique ('radar swath imaging'), explores its methodological principles, describes its operational requirements and highlights recent scientific advances enabled by radar swath imaging. Observations of glacier and substrate morphology and physical properties inferred from swath data have already been used to improve our understanding of ice-shelf melt, basal sliding and subglacial sediment and water transport. Lessons learned from these initial surveys should inform future data collection strategies, so that

THE ROYAL SOCIETY PUBLISHING

radar swath imaging can be deployed in the most productive way possible during upcoming major field campaigns, including the Fifth International Polar Year and beyond.

This article is part of the Theo Murphy meeting issue 'Next generation ice-sheet bed measurements'.

1. Introduction

Radio-echo sounding (RES) has been instrumental in glaciological research since the 1960s, facilitating the mapping of ice sheets and the characterization of their basal conditions [1]. Despite its widespread use, RES has produced a somewhat limited picture of the Antarctic and Greenland Ice Sheets. This is, in part, due to an inherent disparity in the density of sampling along- and across-track when collecting data using conventional RES methods. Radar systems collect data with very fine resolution along profiles (with samples every approx. 1 m), but the spacing between profiles is typically three orders of magnitude larger (with lines spaced every 1–10 km). As a result, digital elevation models (DEMs) of subglacial topography derived from radar data are usually degraded to some resolution between the along-track and across-track spacings, with information lost during the gridding process [2]. Such gridded datasets have proven incredibly valuable for catchment-scale studies, capturing the long-wavelength topography and (in some cases, e.g. [3]) the statistical character of the bed, but they fail to reproduce the true topography at metre scales, limiting what is possible for local ice-flow modelling and process studies.

Radar hardware advancement over the last 20 years has improved data quality, and accompanying developments in signal processing have made it possible to reduce the disparity in along- and across-track resolutions. Multichannel radar systems (designed to see through thick, warm ice) have seen widespread use to map ice thickness. These systems transmit from multiple antenna elements simultaneously to generate a downward-focused beam. Separately recording backscattered energy with each element in the array enables direction-of-arrival (DoA) analysis (or beam forming) in the cross-track direction during post-processing [4] and the unique determination of scatterer position perpendicular to the profile direction. When single-channel radar profiles are collected with sufficient density, this type of target discrimination can be accomplished with three-dimensional migration methods, full-waveform inversion or downward continuation, as has been demonstrated using data collected from Martian orbital radar [5]. But multichannel radars enable this with a single pass. We call this type of data collection (analogous to multibeam sonar imaging) 'radar swath imaging', the data generated by these systems 'radar volumes', and the systems capable of this data collection 'swath radars'.

Since its first proof of concept in [4,6,7], radar swath imaging has yielded maps of alpine glacial valleys [8], ice shelves [9] and ice-sheet subglacial topography at unprecedented resolution [10–12]. This paper deconstructs the data collection and processing workflow for the generation of radar volumes (outlined in figure 1) and presents an overview of the capabilities and limitations of swath radar systems, the possible applications of radar volumes in glaciology and considerations for future survey design and software development to enhance future imaging capabilities.

2. Principles of radar swath imaging

RES involves the transmission, scattering and measurement of electromagnetic waves. Radar hardware transmits an electromagnetic pulse and records a time series of the amplitude and phase of the local electric field, capturing energy scattered in the subsurface returning to the system with a time delay defined by the range to the scattering target. While the goal of RES is to reconstruct the geometry of features in the subsurface, this is an underconstrained problem when range is the only observable (i.e. without knowledge of the DoA for backscattered energy). Below, we lay out

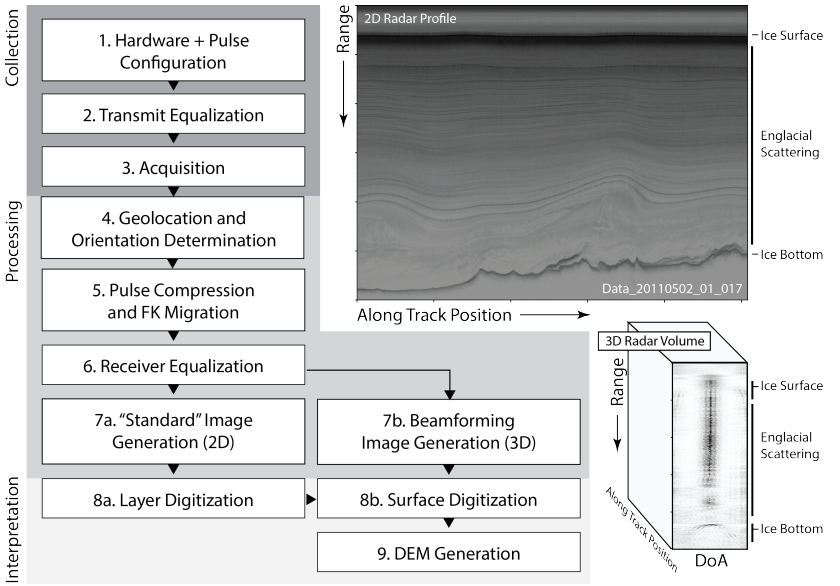

Figure 1. Typical workflow to derive high-resolution digital elevation models (DEMs) of the bedrock topography (described in §2), with examples of conventional, two-dimensional radar data products and three-dimensional swath radar data products. Three-dimensional radar volumes capture the intensity of subsurface backscattering as a function of along-track position, range to the target, and the direction of arrival (DoA) for returning energy. Example radar data presented are from Northern Greenland (frame 20110502_01_017) available from the Open Polar Server [13].

some of the fundamental concepts in geophysical imaging that allow for the unique determination of scattering target locations, and through that, radar swath imaging.

Ice-penetrating radars collect a series of backscattering measurements along profiles, with each acquisition separated from the previous one in space and time. By assuming that scattering targets are stationary, it is possible to use this sequence of measurements to solve for the along-track DoA (described in terms of an 'azimuth angle') for backscattered energy. While this resolves features in the along-track dimension, it does not enable target discrimination in the cross-track dimension. The number and configuration of antennas used for data collection dictate whether or not radar swath imaging (determination of the DoA, or 'elevation angle', in the cross-track direction) is possible. Radar swath imaging requires a multichannel array, consisting of multiple antennas arranged perpendicular to the profiling direction.

Simultaneously transmitting from multiple antennas in a linear cross-track array results in a wave field characterized by constructive and destructive interference that varies as a function of angle. The directions with the greatest constructive interference (described as the 'main lobe') are perpendicular to the linear array, which for typical ice-penetrating radar, maximizes transmit power at nadir. The wider the array, the narrower the main lobe. For off-nadir directions, the nature of the interference and the integrated signal varies as a function of angle, resulting in radiation (or 'beam') patterns that exhibit 'side lobes': directive beams at wider angles separated by destructive interference nodes.

The array size and element density control two critical features of the beam pattern of an array: (i) the main beamwidth and (ii) the amplitude of undesirable off-axis 'grating lobes'. The effect of changes in array configuration on these two properties is shown in figure 2. The beamwidth depends on the 'electrical width' of the array: the ratio of its physical length to the wavelength of the transmission. Electrically narrow arrays result in a wider beam and coarser cross-track resolution (figure 2A). Grating lobes arise when the spacing between elements in the array is greater than one half-wavelength, and they introduce ambiguity between signals in the main beam and those

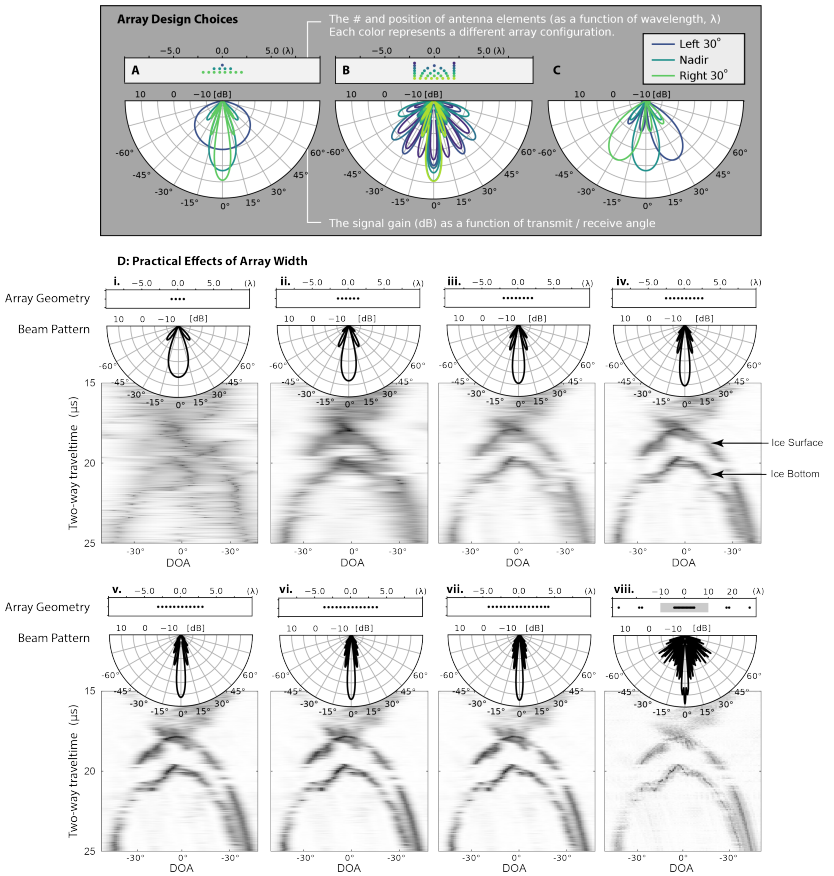

Figure 2. Figures describing the theoretical (A–C) and practical (D) implications of array design for radar swath imaging. In this figure, array geometries show the position of individual antenna elements in a linear array (measured in number of wavelengths from the array centre line, λ). The associated beam patterns show the signal gain due to the combined effects of an individual element's radiation pattern (an example of which is shown in the blue pattern on panel A) and the destructive and constructive interference from simultaneous transmission or recording across the full array. Panel A shows the effect of increasing array width, which narrows the main beam. Panel B shows the effect of increasing array density, which reduces the influence of off-nadir grating lobes. Panel C shows the effect of introducing ramped phase delays across the array, which change the direction of the main beam. Panel D (i–viii) shows the practical effect of changing the array width on the resultant cross-track, DoA images. These images were generated using data collected from subsets of the UHF-COLDEX array flown during the 2023-24 Antarctic NSF COLDEX field season. Increasing the array width (primarily) and number of elements in the array (secondarily) improves scattering target discrimination. Data products were generated for the data frame 20240112_09_022, available through the Open Polar Server [13].

off-axis (figure 2B). Radar swath imaging quality improves when arrays are electrically wide and sufficiently dense to eliminate grating lobes.

By systematically introducing phase delays between antennas in an array, the pattern of interference changes, and it is possible to direct (or 'squint') the main lobe of the beam pattern (figure 2C). When phase delays are applied at transmission, radar systems can illuminate and measure features in only one target direction. The same concept (combining signals with structured phase delays) can be applied to the received signals, such that returning energy from some angles is amplified and energy from other angles suppressed, a technique called 'delay-and-sum beam forming' in the time domain and 'Doppler focusing' in the frequency domain [14]. This is one strategy for producing a three-dimensional radar volume using a cross-track array. Two-dimensional images, each squinted in a different direction using delay-and-sum beam forming,

can be stacked into a three-dimensional radar volume, and scattering events within the volume can be used for swath imaging. While this is not the most common approach for radar volume generation, it provides useful intuition for the structure of radar volumes like those presented in figure 2D. Using data collected in East Antarctica from a 22-channel array flown as part of the National Science Foundation Centre for Oldest Ice Exploration (NSF COLDEX, [15]), we produced cross-track DoA images with a variety of different arrays to demonstrate the effect of array size on image quality. The results, presented in figure 2D(i–viii), demonstrate the practical effects of array width and density on cross-track DoA determination, which we use to make recommendations for future systems and surveys in the following section.

3. System and survey design considerations

Multichannel radar systems capable of swath imaging have been deployed on a number of different airborne and ground platforms, with a variety of array sizes, transmit pulse characteristics and survey geometries. Each instrument and survey choice has implications for the scientific utility of the data collected and should be considered when planning a field campaign. We discuss some of the most effective trade-offs in the following sections.

(a) Transmit configuration

The optimal transmit characteristics differ for swath imaging and conventional profiling, and thus, the first step in radar swath imaging is optimizing the hardware and transmit pulse characteristics for the measurement objective (figure 1 (1,2)). As described above, arrays are most effective at discriminating between scattering targets in the cross-track dimension when they are dense and electrically wide. However, higher frequencies (which allow for physically small but electrically wide arrays) tend to have lower penetration through ice, making full-ice-thickness sounding and swath bed mapping difficult. The bandwidth, which defines the range resolution of the system, also has implications for swath generation. Some cross-track image synthesis approaches require the array be 'narrowband'; that is, arrivals from individual targets of interest, measured across the array, must appear in the same range bin. For 'wideband arrays' (which are long relative to the range resolution), coregistration of images from different antenna elements may be impossible without reducing the angular extent of the scatterers resolved [16]. This represents the first set of trade-offs between nadir imaging priorities (which, to a point, benefit from wider bandwidth and therefore range resolution) and swath imaging priorities (which benefit from electrically wide but narrowband arrays).

Transmitting using all antenna elements across a wide cross-track array produces a narrow but intense beam, which will enhance the signal-to-noise ratio (SNR) for nadir targets but fail to illuminate the off-nadir targets used to construct the swath topography. There are two transmit-pulse strategies that are used to address this issue when attempting to produce three-dimensional radar volumes. The first is simply transmitting from a narrow subset of the array, resulting in a wide but weak transmit beam. Alternatively, data can be collected using a sequence of distinct transmit pulses. By transmitting using all antennas multiple times, with appropriate phase delays to generate a different beam direction for each pulse (e.g. a left-, down- and right-pointing beam), it is possible to maximize total transmit power output without sacrificing angular coverage. To transmit multiple directed beams requires high phase precision across the array, and therefore, careful transmit calibration either in the lab (by measurement of electrical path lengths to each transmit element with a network analyser) or in the field (by transmitting out of each antenna element individually and recording scattering using a single receive element to determine transmit phase offsets).

Each transmit strategy has advantages and disadvantages, but both will degrade the SNR for nadir targets relative to conventional nadir-only imaging. The former, transmitting from a small sub-array, has the advantage of being operationally simple. But it can reduce the SNR of the data

by two mechanisms: radar hardware may limit the total power transmitted from a sub-array (when compared to transmit power from the full array) and the antenna gain associated with the more directive beam is lost. For example, if only one of N transmit elements is used, the total transmit power may be reduced by a scaling factor of $1/N$ (depending on hardware architecture). The change to antenna gain will produce another $1/N$ scaling, resulting in a $1/N^2$ SNR drop. The latter strategy, transmitting a sequence of directed beams, is operationally more complex but has advantages over using a single sub-array. The reduced beamwidth usually results in the illumination of fewer scatterers per pulse, which leads to improved angular estimation [16]. In addition, this strategy may result in a smaller reduction in SNR relative to the sub-array approach. The time-integrated power transmitted in any one direction will still be a fraction of what it would be without the multipulse sequence, but if N beams are used, the total SNR will drop by only a factor of $1/N$. When the system characteristics allow, we recommend the use of directive beams to illuminate off-nadir targets rather than wide-beam, low-power transmission.

Finally, some limitations of the array design can be overcome by modification of the transmit pulse sequence. Each transmit antenna and receive antenna pair contributes to the characteristics of the array; functionally, the number of measurements made by the array is the product of the number of transmit pulses and the number of receivers, with the apparent phase centre of each measurement being the weighted mean position of the transmit and receive antennas used. For systems with significant grating lobes owing to an insufficiently dense physical array, it is possible to increase the effective array density by transmitting a sequence of pulses from different physical positions within the array. This approach, colloquially called 'ping-pong transmission', improves DoA determination at the cost of decreased SNR (again, scaling transmit power by a factor of $1/N$, where N is the number of distinct pulses). Arrays should aim to be greater than five wavelengths wide and satisfy the element spacing requirements (less than 1/2 wavelength) to minimize grating lobes; ping-pong transmission should therefore only be used when the physical array does not meet these requirements.

(b) Logistics costs

Multichannel systems require more resources than single-channel systems. They can be heavier, they can require more space and power, and they can have higher data rates, requiring robust onboard storage and channel synchronization mechanisms. Antenna integration is also more complicated owing to the additional antenna elements. However, the specific costs associated with these systems are ultimately dependent on system architecture (e.g. increasing transmit power increases the weight, cross-polarimetric antennas are heavier and generally less aerodynamic, system centre frequency changes antenna size and fairing configuration, and system bandwidth affects total data volume) and therefore must be considered on a mission-by-mission basis.

Weight and power requirements are particularly important to consider as low-power or low-logistics platforms for radar sounding, such as uncrewed aerial vehicles (UAVs), become more widespread [17,18]. Past swath radar campaigns have not been power limited, but some did use heavy electronics and antennas that reduced platform range. Recent engineering work has focused on reducing weight. For example, Won *et al.* [19] demonstrated broadband (170–470 MHz) open-sleeve dipole antennas weighing only a few pounds, and later 32 of these antennas were integrated on a Basler aircraft without the need for custom hardpoints because of their lightweight aerodynamic design. Based on Arnold *et al.*'s [20] recently developed four-channel CReSIS UAV radar, the electronics for an eight-channel system with 800 W peak transmit power would weigh about 15 kg, consume 80 W for the digital system and receivers, and consume transmit power ranging linearly from 20 to 200 W for duty cycles ranging from 1 to 10%. Single or multichannel systems of this weight class would result in essentially no change in range for crewed aerial platforms.

In contrast with swath imaging from crewed vehicles, multichannel imaging via UAVs is confounded by the platform size. Smaller UAVs, such as quadcopters, are unlikely to be able to

support a swath very-high-frequency system, although it may be possible to combine some platforms in a multistatic radar set-up to achieve swath processing. Even larger UAVs, such as the Windracers ULTRA MK2, would suffer range reductions owing to the extra weight and antenna drag of existing swath-capable systems, so at present, we consider operation most feasible on crewed aircraft or ground missions.

system, although it may be possible to combine some platforms in a multistatic radar set-up to achieve swath processing. Even larger UAVs, such as the Windracers ULTRA MK2, would suffer range reductions owing to the extra weight and antenna drag of existing swath-capable systems, so at present, we consider operation most feasible on crewed aircraft or ground missions.

(c) Survey design and platform selection

Because swath systems are defined by their angular resolution (rather than a fixed cross-track spatial resolution), increases in range to the target will result in increased swath width but decreased lateral resolution. High-altitude airborne platforms can produce wide swaths of topography at the cost of coarser cross-track resolution. When the project objective is to produce a seamless DEM, flights should be collected no further than 2 km apart when flying at standard acquisition altitude (between 100 and 1000 m above the ice surface) for typical ice thickness (greater than 1000 m), assuming otherwise ideal imaging conditions.

Ground-based systems have advantages and disadvantages, all a product of travelling slowly and coupling directly to the snow, firn, or ice. Airborne platforms lose angular coverage due to refraction at the air–ice interface, which functionally restricts downgoing angles to less than 34° (the critical angle for radio waves in ice). By coupling to the surface, ground-based systems experience reduced refractive effects but have difficulty collecting data where the surface is too soft, where the surface is too hard, or in crevassed terrain. Their slower platform speeds (less than 10 km h^{-1}, compared with airborne speeds between 200 and 600 km h^{-1}) allow for improved SNRs via averaging in hardware but reduce daily coverage, restricting collection to smaller areas. For targeted surveys, especially in regions with high relief, steeply sloping englacial layers or high loss ice, ground surveys will produce better results than airborne surveys and should be considered.

Where the subglacial topography is smooth, scattering from off-nadir can be weak or nonexistent. Because subglacial topography tends to be smoother in the ice-flow direction than across the ice-flow direction, to maximize the signal in cross-track images, profiles should be collected along flow when radar swath imaging is a primary survey goal. This has the added benefit of providing stratigraphic measurements that are more easily linked to ice-flow models [21].

4. Data processing

Generating three-dimensional radar volumes requires precise position information and phase calibration, synthetic aperture radar (SAR) processing, and DoA determination. Once three-dimensional radar volumes are generated, two-dimensional surfaces must be extracted by either manual or automatic data annotation. The typical processing and interpretation workflow (currently implemented in the Open Polar Radar Toolbox) is outlined in figure 1 (4–9).

Processing starts with analysis of data collected by global navigation satellite system receivers and inertial navigation systems, which provide precise geolocation and motion compensation for coherent SAR processing. Then, time and phase differences for each channel that arise from system characteristics (inherent to the radar hardware) must be determined and corrected for. Like transmit equalization, receive equalization can either be done in the lab or corrections can be generated empirically from field measurements.

For near-nadir targets, the phase differences measured between elements in the array can be explained by (a) system effects (unique to each of the N channels) and (b) the incoming, cross-track DoA for the energy. This yields a total of $n + 1$ unknowns required to explain the N measurements. If one assumes that a scattering target is exactly at nadir, any measured phase differences must be

entirely due to system characteristics, which can then be removed. In circumstances where the target position is unknown, it is possible to use multiple targets to uniquely determine the scattering direction and phase equalization coefficients across the array. Every target with a distinct arrival angle near nadir adds one new unknown (the DoA to that target) and N more measurements, allowing for the unique determination of phase delays in the system. This type of receiver equalization is conventionally performed using data from the beginning of each season and updated whenever the hardware configuration is altered.

For targets arriving from wide angles, phase differences measured across the array can deviate from the expected phase ramp, largely due to interference between the direct arrival of backscattered energy and near-field reflections of that energy from the ground plane (in the case of airborne systems, typically the wing or fuselage). Data collection over known, static features (e.g. the ocean surface or rock surfaces for which there are independent DEMs) can be used to perform array manifold (or 'steering vector') calibration. This is the empirical determination of system-induced, DoA-dependent deviations from the expected phase in measurements across the array. Datasets collected in the Canadian Arctic show significant position errors for targets more than 50° off nadir when no steering vector calibration is applied, resulting in a characteristic but erroneous upward curvature ('smiling') to the swath topographies [16]. For surveys with complex antenna fairings intending to use the wide-angle measurements, steering vector calibration is a necessary step.

Once receiver equalization, steering vector calibration and SAR focusing are complete, three-dimensional images can be generated. Delay-and-sum beam forming [22], periodogram, minimum variance distortionless response and MUltiple SIgnal Classification (MUSIC) algorithms (all found in [23]) and maximum likelihood estimation approaches [7] have each been applied to multichannel radar data to perform cross-track DoA determination. All of these algorithms generate three-dimensional volumes which reveal both the qualitative nature of subsurface scattering and the precise location of subsurface targets. In these volumes, rough interfaces (such as the ice-sheet surface and ice-sheet bed) act as multiple scattering targets and backscatter across a range of angles, producing traceable horizons in cross-track slices of the radar volume. By digitizing those horizons and using time-of-flight information for the backscattered energy, it is possible to reconstruct the geometry of the interface in three-dimensional space, converting from two-way travel time and DoA to $x/y/z$ position, accounting for refraction across the ice–air interface.

The implementation of the MUSIC algorithm and the sequential tree re-weighted (TRW-S) auto-annotation scheme in the Open Polar Radar Toolbox has been widely used to generate swath topographies (e.g. [8–12]). This approach has strengths and weaknesses. The MUSIC algorithm generates the best scatterer localization when the number of targets is small relative to the number of independent measurements (described by [4], referencing [24]). But the MUSIC volume does not directly reflect the amplitude of the cross-track scattering, so while it produces high-quality target locations, it cannot be used for amplitude analysis. Future work, focused on radiometric properties rather than subsurface geometry, should further explore the other beam forming techniques, which preserve amplitude information from the original data.

TRW-S is one of a very small number of implemented auto-annotation schemes. At its core, it solves an optimization problem designed to generate surfaces that closely follow maxima in the intensity of the three-dimensional radar volume, regularized by along- and cross-track smoothness parameters and surface slope expectations [25]. Unconstrained, the TRW-S algorithm has difficulty reproducing the true surface in the data volume. In practice, then, surface extraction requires the manual generation of ground-control points to improve algorithm performance, a labour-intensive task. But once complete, swath DEMs can be used for a variety of scientific applications, described below.

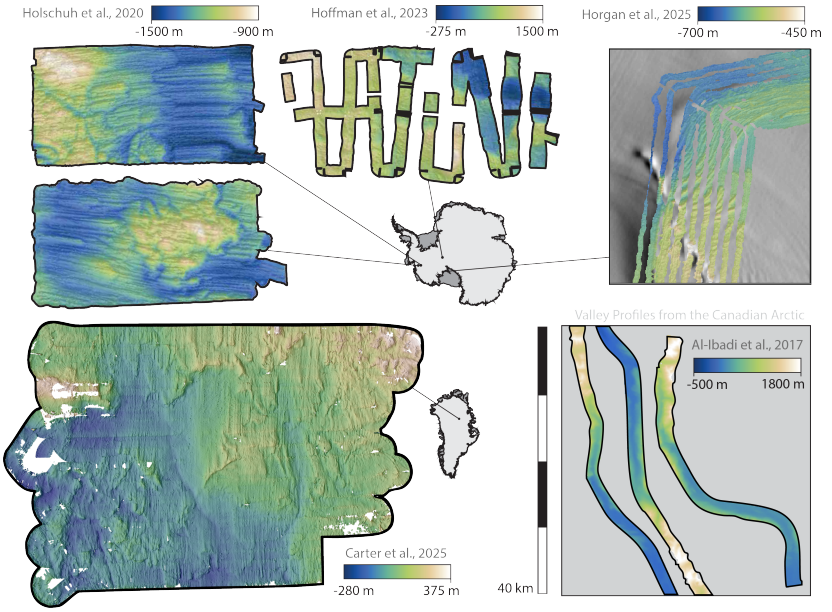

Figure 3. Compilation of swath DEMs from [8–12], presented at equal horizontal scale but different vertical scale. This figure captures the diverse textures revealed by radar swath imaging in ice-sheet interior sites (left and centre columns), at ice-sheet grounding zones (top right), and in alpine glacier valleys (bottom right).

5. Published applications of three-dimensional radar volumes and swath topographies

Where they have been collected and processed, three-dimensional radar volumes have been used creatively to better understand ice-flow processes and ice-sheet history. Continuous, fine-resolution DEMs have been produced for parts of Thwaites Glacier [10] and the onset of the Northeast Greenland Ice Stream [12], and individual swaths have been produced and interpreted at Hercules Dome [11], the grounding line of Kamb Ice Stream and the Ross Ice Shelf [9] and in the Canadian Arctic [8] (figure 3). In addition, new data have been collected over Thwaites Glacier, the East Antarctic Plateau, the Ross and McMurdo Ice Shelves and in coastal Dronning Maud Land for the purpose of radar swath imaging. As the quantity of radar swath data collected grows, novel applications of these data emerge. Here, we describe some of the ways swath data have been used to date and provide suggestions for their future application.

With the first regional DEM generated using radar swath imaging, Holschuh *et al.* [10] demonstrated that swath radar can map the glacier subsurface at resolutions comparable to modern DEMs of other terrestrial environments. This naturally led to comparisons between subglacial and postglacial landscapes, and thus, radar swath topographies have been used to improve our understanding of glacial geomorphology. By resolving bedform orientations and shapes across broad areas under Thwaites Glacier, Holschuh *et al.* [10] were able to test models of bedform generation published in the glacial geology literature. The swath data led to two important discoveries:

- Fine-resolution DEMs allowed for detailed water-flow routing, producing water pathways that are orthogonal to the ice-flow direction. The orientation of bedforms is consistent with ice-flow direction but not water-flow direction in the region, indicating they are probably formed by sediment transport by ice and not by water (following the rilling hypothesis) proposed for some elongate subglacial bedforms (e.g. [26]).
- The size distribution of bedforms is weakly correlated with the basal shear stress in the region, and when compared with co-located seismic data, it is apparent that the presence

of bedforms is itself indicative of substrate material strength [27]. That discovery implies radar swath-derived DEMs could be used to infer material properties using geomorphological indicators and constrain spatial variability in model-implemented sliding laws or basal friction coefficients.

Radar swath imaging of the bed at the onset of the Northeast Greenland Ice Stream (NEGIS) by Carter *et al.* expanded on this work, revealing the basal conditions of the ice stream as well as its past ice dynamics [12]. Mega-scale glacial lineations (MSGLs) were identified far into the interior of the ice sheet (approx. 600 km upstream of the grounding line), forming beneath relatively slow-flowing ice. This was a surprising result; preceding the publication of the data at NEGIS, MSGLs had only been observed in areas with ice velocities greater than 100 m $year^{-1}$, closer to the termini of Rutford Ice Stream [28,29] and Thwaites Glacier [10]. The inference that these MSGLs probably formed *in situ* under modern-day slow ice velocities (less than 60 m $year^{-1}$) questions the paradigm that MSGLs are exclusively associated with fast ice flow [12].

Previous studies of NEGIS inferred saturated, high-porosity, deforming sediments across the region around the EastGRIP drill site from seismic data analysis [30,31]. This interpretation became more nuanced after swath radar data collection, as the landscape revealed by the high-resolution DEM implies a mixed bed assemblage, comprising both hard bedrock outcrops and softer sediments, comparable to paleo-ice stream beds in the North Sea [32]. Crag-and-tails identified beneath very slow-flowing ice, outside of the current shear margins of the NEGIS, also suggest a potential spatial evolution of the north-western shear margin, as the elongation of these landforms would indicate that they experienced streaming flow conditions at some point in the past [12].

Even without seamless regional DEMs, individual radar swath topographies have been used to understand the statistical character of the ice-sheet bed, and through that, make inferences about substrate material properties and the glacier flow regime. At Hercules Dome, individual swath DEMs show elongate bedforms within major topographic troughs in the region [11]. These bedforms are not oriented parallel to the modern ice-flow direction, but rather, are parallel to the trough axis. These data were used to infer the presence of soft sediment in the valley troughs, corroborated by regional gravity surveys, and establish the paleo ice-flow conditions (streaming flow parallel to the trough axis), which together have implications for the dynamics of ice-sheet regrowth following deglaciation of West Antarctica [11].

At the grounding zone of Kamb Ice Stream, individual swaths capture the morphology of a major (200 m tall) subglacial channel that drains into the cavity under the Ross Ice Shelf [9]. These data reveal both large-scale continuity of the channel into the ice shelf and complexity in its morphology downstream, with lateral offsets and apparent changes in channel depth (probably associated with time-varying discharge). They also expose grounding-zone parallel ridges that probably reflect periodic variations in basal melt or ice discharge rates where the ice goes afloat. With precise estimates of channel volume and shape, swath data enable better melt-rate estimation and plume or cavity circulation modelling for this system.

While prognostic modelling using the full resolution of swath-generated DEMs has not yet been performed, targeted diagnostic modelling experiments have been conducted using the DEMs generated for Thwaites Glacier. The goal of the study by Hoffman *et al.* [33] was to determine whether or not 25 m resolution DEMs were sufficient to capture the majority of the system's form drag (the resistance to ice flow induced by the macroscale morphology of the ice base, separate from skin drag, the inherent strength of the interface between ice and rock). This work shows that, on average, reproducing the observed velocity with smoother topography (such that it no longer captures the shortest-wavelength features) requires artificially higher stresses at the model's interface between ice and rock. But the change in skin drag due to topographic smoothing was not uniform across the Thwaites domain. Where the bed was roughest as observed by the swath radar (corresponding with the regions thought to be bedrock based on collocated seismic data [27]), resistance to flow at the interface was high and less sensitive to smoothing. A conclusion of Hoffman *et al.* [33] was that 25 m resolution DEMs are still insufficient to capture all of the

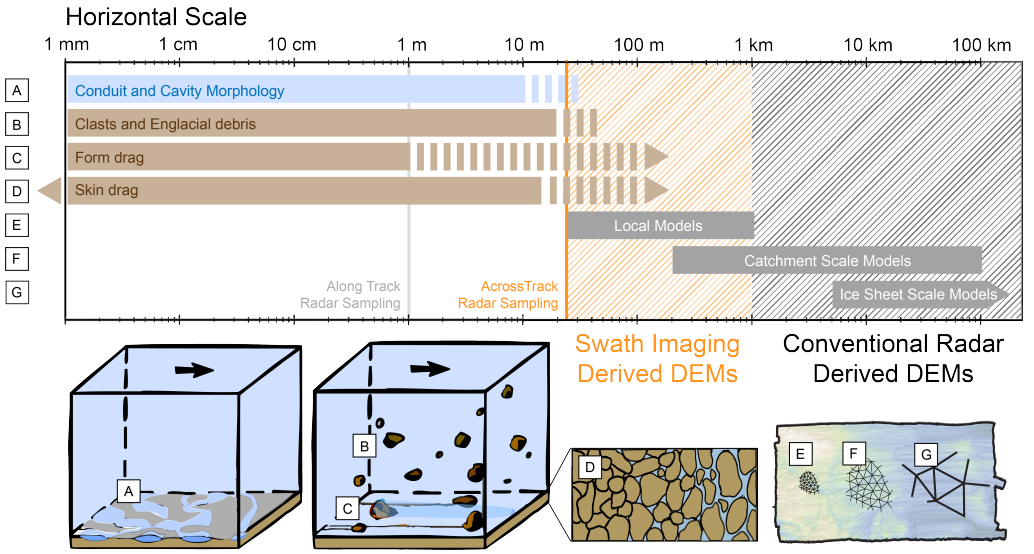

Figure 4. A summary of the horizontal spatial scales for the processes and properties that govern basal drag, typical model resolution and the resolution of radar-derived observations (both profiles and gridded products). Schematic diagrams highlight controls on basal drag, including (A) the effective contact area between ice and rock controlled by the configuration of subglacial hydrologic system, (B) resistance to flow associated with englacial debris, (C) form drag due to regelation and enhanced creep around bed topography and (D) skin drag due to changes in sediment pore pressure. Swath radar data bring the resolution of DEMs (hatched in grey and orange) closer to the scale used by local models (E, e.g. [34,35]), to the scale required for mesh refinement at the edges of catchment-scale models (F, e.g. [36,37]) and to finer resolution than current continental-scale models of ice flow (F).

features relevant to the ice-sheet stress balance, but they can be used to evaluate local sensitivity to errors in the prescribed topography. As the ice-sheet modelling community works to include time-evolving bed friction in ice-sheet models, it becomes increasingly important that we develop observational methods capable of separating the (time-dependent) interface properties from the (static) morphological components of drag. In addition, Hoffman *et al.* [33] show how swath topographies capture the two-dimensional spectral character of the bed, which may be useful for inferring sub-resolution features (and, critically, their orientation) for use in analytical calculations of form-drag at all scales.

6. Future applications

Radar swath imaging extends the fine resolution of one-dimensional profiles to the cross-track dimension, providing some of the first, entirely data-derived representations of the ice-sheet bed with the scale and coverage required for fine-resolution ice-sheet modelling. These data have begun to address two major goals within the glaciology community:

(i) *Close the model resolution-observation gap*: reduce the discrepancy between the finest resolution numerical models and the resolution and coverage of observational boundary conditions employed by those models.
(ii) *Close the process-observation gap*: define unresolved processes that affect ice flow and develop measurement concepts that can inform their implementation in ice-sheet models.

Historically, the scale at which glaciological processes play out at the ice-sheet base, the scale at which we represent ice sheets in models, and the scale at which we have measured real ice-sheet systems have been vastly different (figure 4). If our goal is to close the gap between process, model and observation by generating spatially complete knowledge of the ice-sheet bed, it will require

collecting more and new types of data. The utility of radar swath imaging in accomplishing this goal will depend on how future data are collected; individual profiles with locally fine resolution but incomplete coverage have different applications than continuous regional surveys. We provide a vision for each of these data collection approaches below.

It is possible to produce DEMs with uniform, 25 × 25 m resolution using radar swath imaging when radar volumes are overlapping. That requires line spacing that is narrower than the swath width, coverage that is as dense or more dense than typical surveys collected in the last 20 years. Resolution refinement in models is prioritized (i) at and upstream of the grounding zone of marine-terminating glaciers and (ii) in other areas of fast flow where complex subglacial heterogeneity in ice-sheet properties affects the stress balance. High-resolution DEMs of ice shelves can also help inform models of sub-ice-shelf circulation and subglacial discharge. As a result, radar swath imaging as part of initiatives like Antarctic RINGS [2], which target these dynamic areas, will bring the greatest benefit, assuming attenuation and scattering allow for deep imaging near the grounding zone. However, without 2–5 km line spacing everywhere in Antarctica and Greenland, radar swath imaging is not itself a solution to the problem of improving continental-scale data products, required for accurate projection [38,39].

As an alternative strategy to dense data collection, disjoint swaths can be collected and used to improve interpolated data products. Packages like GStatSim [40] use the statistical character of the bed to improve interpolation, and individual swaths capture multidimensional statistics of the bed, exposing variability and local anisotropy in bed topography that can be used both as part of the statistical input to kriging interpolation (improving the variogram used to define observational weights) and to identify abrupt changes in the statistics of the landscape to inform piecewise interpolation strategies. While relying on interpolated products will still result in some of the same loss of information and reduction in resolution that occurs when interpolating profiling radar data, products informed by individual swaths have the potential to have higher fidelity when compared with the true topography than interpolated products only informed by profiles, as they contain multidimensional statistics that profiles do not. More work is needed to understand where 'realistic' but not 'real' boundary conditions are sufficient for modelling, to motivate this style of survey rather than seamless DEM production.

'Glacier sliding' is a parameterized process that represents the integrated effects of englacial debris [41], fine-scale bed roughness [42,43], substrate material strength [44–48], cavitation [49–53] and effective pressure [54,55] on the glacier stress balance (figure 4). It is unlikely that observations will ever capture everything required to model glacier sliding at true scale across ice-sheet catchments, raising questions about how observations should inform the way we implement sliding parameterizations. Hoffman *et al.* [33] show that the spectral character of resolved roughness may tell us about features below the resolution of swath radar, and Muto *et al.* [27] show that the qualitative nature of bed features may reflect substrate material properties. Spectral analysis of swaths combined with inferred material properties from morphological differences could therefore be used to generate bed topographies that are realistic in all orientations, producing boundary conditions that are more robust to changing flow conditions than those generated using only along- and across-flow profiles corresponding to the modern flow field. More work spanning the field and lab should be done to expand the range of inferences made possible using profiling and swath radar.

In addition to their use in DEM generation, radar volumes have the potential to improve the way we interpret the structure and properties of the ice itself [56]. Most englacial scattering arises from stacked specular interfaces. As a result, only one englacial target is typically observed per range shell within the three-dimensional radar volume (as seen in the radar volume shown in figure 1). In some places, however, englacial scattering appears diffuse, with targets arriving from multiple angles within the same range shell. This probably occurs where there is entrained debris [57], englacial melt water or gradual transitions in the ice crystal fabric, resulting in volume scattering [58]. When combined with polarimetric radar, three-dimensional radar volumes could

help us understand the complex nature of scattering in complex basal ice, which has been a source of uncertainty in ice-core site selection surveys over the past decade [59].

Finally, the DoA associated with scattering from specular layering within the ice sheet can inform analysis of ice deformation. When combined with along-track slopes derived from SAR processing, the surface normal for englacial layering can be measured, allowing the true layer slope magnitude and direction to be determined. This could be used to better understand the integrated history of deformation that produced the sloping layers [21]. Measurements of layer slopes also enable repeat-track interferometric processing of profiling radar data. Radar interferometry uses phase differences between radar measurements taken at the same place at two different times to infer how the subsurface geometry is evolving. But slight errors in the position of the radar during the two acquisitions, leading to a non-zero spatial baseline, can induce significant phase changes independent of subsurface deformation. Knowledge of the three-dimensional layer geometry makes it possible to correct for this error in phase and directly measure subsurface strain using repeat radar measurements [60].

7. Conclusions

Radar swath imaging is a valuable new tool for the study of ice sheets, generating data that can be used to measure three-dimensional ice-sheet geometry, understand ice-shelf melt, infer substrate material properties, test models of landform development and improve projections of future glacier change. As planning progresses for the major field campaigns of the coming decade (e.g. Antarctica InSync and the Fifth International Polar Year), radar swath imaging should be considered for areas where fine resolution mapping will have the most value. This includes current and future ice-sheet grounding zones, dynamic ice shelves, areas of fast flow with high subglacial relief and regions that are presently slow-flowing but were subject to faster flow in the past. In addition, targeted surveys capturing a range of glaciological environments not already sampled by swath radar have the potential to transform our understanding of subglacial erosion, deposition, glacial geomorphology and englacial properties (crystal-orientation fabric and englacial debris entrainment). While radar swath imaging has limitations (e.g. more stringent platform requirements, higher weights, implications for power draw and data storage needs and dense line spacing requirements for continuous coverage), it provides a novel view of ice-sheet structure and subglacial environments and will contribute significantly to the way we map ice sheets and glaciers over the coming decades.

Data accessibility. Radar data processing and analysis were performed using tools developed as part of Open Polar Radar, https://gitlab.com/openpolarradar/opr/ [61]. Data products (presented in figure 2) and example processing code (which can be used to reproduce the three-dimensional data products provided from SAR focused conventional imagery, available through the Open Polar Server) can be found in the Harvard Dataverse persistent repository with the following citation: [62]. Raw and intermediate data products are available through the Open Polar Radar project—for access to the data server and processing resources, contact: opr@openpolarradar.org. Digital elevation models plotted in this manuscript are available through their source manuscripts.

Declaration of AI use. We have not used AI-assisted technologies in creating this article.

Authors' contributions. N.H.: conceptualization, data curation, formal analysis, funding acquisition, methodology, visualization, writing—original draft, writing—review and editing; O.E.: conceptualization, funding acquisition, project administration, supervision, writing—review and editing; C.C.: visualization, writing—original draft, writing—review and editing; S.F.: writing—review and editing; V.H.: writing—original draft, writing—review and editing; A.H.: visualization, writing—original draft, writing—review and editing; J.P.: conceptualization, funding acquisition, software, writing—review and editing; K.C.: conceptualization, funding acquisition, writing—review and editing.

All authors gave final approval for publication and agreed to be held accountable for the work performed therein.

Conflict of interest declaration. We declare we have no competing interests.

Funding. We would like to thank NASA for support for radar swath imaging work under grant NASA-80NSSC21K0753, and NSF COLDEX for support in data collection and algorithm development under grant

NSF-2019719, and personnel and acquisition support under NSF awards RISE-2126503, OPP-1744649, and EAR-1738934. AWI radar data were supported by logistic grantsAWI_PA_02097 and AWI_PA_02130.

Acknowledgements. We thank the Royal Society for enabling the workshop on 'Next generation ice sheet bed measurements' and travel support for some of the authors. We would also like to thank our two anonymous reviewers for helpful feedback on this work.

References

1. Schroeder DM *et al*. 2020 Five decades of radioglaciology. *Ann. Glaciol*. **61**, 1–13. (doi:10.1017/aog.2020.11)
2. Pritchard HD *et al*. 2025 Bedmap3 updated ice bed, surface and thickness gridded datasets for Antarctica. *Sci. Data* **12**, 414. (doi:10.1038/s41597-025-04672-y)
3. Shackleton C, Matsuoka K, Moholdt G, Van Liefferinge B, Paden J. 2023 Stochastic simulations of bed topography constrain geothermal heat flow and subglacial drainage Near Dome Fuji, East Antarctica. *J. Geophys. Res*. **128**, F007269. (doi:10.1029/2023JF007269)
4. Paden J, Akins T, Dunson D, Allen C, Gogineni P. 2010 Ice-sheet bed 3-D tomography. *J. Glaciol*. **56**, 3–11. (doi:10.3189/002214310791190811)
5. Foss FJ, Putzig NE, Campbell BA, Phillips RJ. 2017 3-D imaging of Mars' polar ice caps using orbital radar data. *Lead. Edge* **36**, 43–57. (doi:10.1190/tle36010043.1)
6. Jezek K, Wu X, Gogineni P, Rodríguez E, Freeman A, Rodriguez-Morales F, Clark CD. 2011 Radar images of the bed of the Greenland ice sheet. *Geophys. Res. Lett*. **38**, 1–5. (doi:10.1029/2010GL045519)
7. Wu X, Jezek KC, Rodriguez E, Gogineni S, Rodriguez-Morales F, Freeman A. 2011 Ice sheet bed mapping with airborne SAR tomography. *IEEE Trans. Geosci. Remote Sens*. **49**, 3791–3802. (doi:10.1109/tgrs.2011.2132802)
8. Al-Ibadi M *et al*. 2017 DEM extraction of the basal topography of the Canadian archipelago ICE caps via 2D automated layer-tracker. In *2017 IEEE International Geoscience and Remote Sensing Symposium (IGARSS)*, Fort Worth, TX, pp. 965–968. Piscataway, NJ: IEEE. (doi:10.1109/IGARSS.2017.8127114)
9. Horgan HJ *et al*. 2025 A West Antarctic grounding-zone environment shaped by episodic water flow. *Nat. Geosci.* **18**, 389–395. (doi:10.1038/s41561-025-01687-3)
10. Holschuh N, Christianson K, Paden J, Alley RB, Anandakrishnan S. 2020 Linking postglacial landscapes to glacier dynamics using swath radar at Thwaites Glacier, Antarctica. *Geology* **48**, 268–272. (doi:10.1130/g46772.1)
11. Hoffman AO *et al*. 2023 Scars of tectonism promote ice-sheet nucleation from Hercules Dome into West Antarctica. *Nat. Geosci*. **16**, 1005–1013. (doi:10.1038/s41561-023-01265-5)
12. Carter CM, Franke S, Jansen D, Stokes CR, Helm V, Paden J, Eisen O. 2025 Formation of mega-scale glacial lineations far inland beneath the onset of the Northeast Greenland Ice Stream. *Cryospher* **19**, 5299–5315. (doi:10.5194/tc-19-5299-2025)
13. CReSIS. 2024 Radar Depth Sounder Data. Lawrence, Kansas, USA. Digital Media. See http://data.cresis.ku.edu/.See: https://data.cresis.ku.edu/, for explanation.
14. Hills BH, Siegfried MR, Holschuh N, Verboncoeur H, Schroeder DM. 2026 Resolving radiostratigraphy with squinted synthetic aperture radar focusing. *J. Glaciol*. **72**, 1–26. (doi:10.1017/jog.2025.10122)
15. Kaundinya S *et al*. 2024 A multi-channel airborne UHF radar sounder system for oldest ice exploration: development and data collection. In *IGARSS 2024 - 2024 IEEE International Geoscience and Remote Sensing Symposium*, Athens, Greece, pp. 41–44. Athens, Greece: IEEE. (doi:10.1109/IGARSS53475.2024.10640448)
16. Moore T, Paden J, Leuschen C, Rodriguez-Morales F. 2022 Nonparametric array manifold calibration for ice sheet tomography. *IEEE Trans. Geosci. Remote Sens*. **60**, 1–20. (doi:10.1109/tgrs.2021.3137145)
17. Teisberg TO, Broome AL, Schroeder DM. 2024 Open radar code architecture (ORCA): a platform for software-defined coherent chirped radar systems. *IEEE Trans. Geosci. Remote Sens*. **62**, 1–11. (doi:10.1109/tgrs.2024.3446368)

18. Ershadi MR, Drews R, Hawkins JD, Elliott J, Lines AP, Koch I, Eisen O. 2024 Autonomous rover enables radar profiling of ice-fabric properties in Antarctica. *IEEE Trans. Geosci. Remote Sens*. **62**, 1–9. (doi:10.1109/TGRS.2024.3394594)
19. Won H *et al*. 2021 VHF/UHF open-sleeve dipole antenna array for airborne ice sounding and imaging radar. *IEEE Antennas Wirel. Propag. Lett*. **20**, 883–887. (doi:10.1109/lawp.2021.3066288)
20. Arnold E *et al*. 2025 A Reconfigurable radar for ice and snow measurements onboard ultra-long endurance UAS: development and flight tests. In *IGARSS 2025 - 2025 IEEE International Geoscience and Remote Sensing Symposium*, pp. 35–39. Brisbane, Australia: IEEE.
21. Holschuh N, Parizek BR, Alley RB, Anandakrishnan S. 2017 Decoding ice sheet behavior using englacial layer slopes. *Geophys. Res. Lett*. **44**, 5561–5570. (doi:10.1002/2017gl073417)
22. Heister A, Scheiber R. 2018 Coherent large beamwidth processing of radio-echo sounding data. *Cryosphere* **12**, 2969–2979. (doi:10.5194/tc-12-2969-2018)
23. Paden J, Allen C, Gogineni P. 2010 3D imaging of ice sheets. In *2010 IEEE International Geoscience and Remote Sensing Symposium*, pp. 2611–2613. IEEE. (doi:10.1109/IGARSS.2010.5649163)
24. Proakis JG, Manolakis DG. 1996 *Digital Signal Processing: Principles, Algorithms, and Applications, 3/e*, p. 07458. NJ, USA: Prentice-Hall International, Inc.
25. Berger V, Xu M, Al-Ibadi M, Chu S, Crandall D, Paden J, Fox GC. 2019 Automated ice-bottom tracking of 2D and 3D ice radar imagery using viterbi and TRW-S. *IEEE J. Sel. Top. Appl. Earth Obs. Remote Sens*. **12**, 3272–3285. (doi:10.1109/jstars.2019.2930920)
26. Fowler AC. 2010 The formation of subglacial streams and mega-scale glacial lineations. *Proc. R. Soc. A Math. Phys. Eng. Sci* **466**, 3181–3201. (doi:10.1098/rspa.2010.0009)
27. Muto A, Anandakrishnan S, Alley RB, Horgan HJ, Parizek BR, Koellner S, Christianson K, Holschuh N. 2019 Relating bed character and subglacial morphology using seismic data from Thwaites Glacier, West Antarctica. *Earth Planet. Sci. Lett*. **507**, 199–206. (doi:10.1016/j.epsl.2018.12.008)
28. King EC, Hindmarsh RCA, Stokes CR. 2009 Formation of mega-scale glacial lineations observed beneath a West Antarctic ice stream. *Nat. Geosci*. **2**, 585–588. (doi:10.1038/ngeo581)
29. Schlegel R, Murray T, Smith AM, Brisbourne AM, Booth AD, King EC, Clark RA. 2022 Radar derived subglacial properties and landforms beneath rutford ice stream, West Antarctica. *J. Geophys. Res*. **127**, e2021JF006349. (doi:10.1029/2021JF006349)
30. Christianson K, Peters LE, Alley RB, Anandakrishnan S, Jacobel RW, Riverman KL, Muto A, Keisling BA. 2014 Dilatant till facilitates ice-stream flow in northeast Greenland. *Earth Planet. Sci. Lett*. **401**, 57–69. (doi:10.1016/j.epsl.2014.05.060)
31. Riverman KL, Anandakrishnan S, Alley RB, Holschuh N, Dow CF, Muto A, Parizek BR, Christianson K, Peters LE. 2019 Wet subglacial bedforms of the NE Greenland Ice Stream shear margins. *Ann. Glaciol*. **60**, 91–99. (doi:10.1017/aog.2019.43)
32. Roberts DH *et al*. 2019 The mixed-bed glacial landform imprint of the North Sea Lobe in the western North Sea. *Earth Surf. Process. Landforms* **44**, 1233–1258. (doi:10.1002/esp.4569)
33. Hoffman AO, Christianson K, Holschuh N, Case E, Kingslake J, Arthern R. 2022 The impact of basal roughness on Inland Thwaites Glacier sliding. *Geophys. Res. Lett*. **49**, e2021GL096564. (doi:10.1029/2021GL096564)
34. Law R, Christoffersen P, MacKie E, Cook S, Haseloff M, Gagliardini O. 2023 Complex motion of Greenland Ice Sheet outlet glaciers with basal temperate ice. *Sci. Adv*. **9**, eabq5180. (doi:10.1126/sciadv.abq5180)
35. Wheel I, Benn DI, Crawford AJ, Todd JA, Zwinger T. 2024 A new 3D full-Stokes calving algorithm within Elmer/Ice (v9.0). *Geosci. Model Dev* **17**, 5759–5777. (doi:10.5194/gmd-17-5759-2024)
36. Lee V, Cornford SL, Payne AJ. 2015 Initialization of an ice-sheet model for present-day Greenland. *Ann. Glaciol*. **56**, 129–140. (doi:10.3189/2015aog70a121)
37. Reed B, Green JAM, Jenkins A, Gudmundsson GH. 2024 Melt sensitivity of irreversible retreat of Pine Island Glacier. Cryosphere **18**, 4567–4587. (doi:10.5194/tc-18-4567-2024)
38. Gasson E, DeConto R, Pollard D. 2015 Antarctic bedrock topography uncertainty and ice sheet stability. *Geophys. Res. Lett*. **42**, 5372–5377. (doi:10.1002/2015gl064322)
39. Sun S, Cornford SL, Liu Y, Moore JC. 2014 Dynamic response of Antarctic ice shelves to bedrock uncertainty. *Cryosphere* **8**, 1561–1576. (doi:10.5194/tc-8-1561-2014)

40. MacKie E, Field M, Wang L, Yin Z, Schoedl N, Hibbs M. 2022 GStatSim (doi:10.5281/zenodo.7274640)
41. Hansen DD, Warburton KLP, Zoet LK, Meyer CR, Rempel AW, Stubblefield AG. 2024 Presence of frozen fringe impacts soft-bedded slip relationship. *Geophys. Res. Lett*. **51**, e2023GL107681. (doi:10.1029/2023GL107681)
42. Weertman J. 1957 On the sliding of glaciers. *J. Glaciol*. **3**, 33–38. (doi:10.1007/978-94-015-8705-119)
43. Kamb B. 1970 Sliding motion of glaciers: theory and observation. *Rev. Geophys*. **8**, 673–728. (doi:10.1029/rg008i004p00673)
44. Iverson NR, Hooyer TS, Baker RW. 1998 Ring-shear studies of till deformation: Coulomb-plastic behavior and distributed strain in glacier beds. *J. Glaciol*. **44**, 634–642. (doi:10.3189/s0022143000002136)
45. Clarke GKC. 2005 Subglacial processes. *Annu. Rev. Earth Planet. Sci*. **33**, 247–276. (doi:10.1146/annurev.earth.33.092203.122621)
46. Damsgaard A, Egholm DL, Beem LH, Tulaczyk S, Larsen NK, Piotrowski JA, Siegfried MR. 2016 Ice flow dynamics forced by water pressure variations in subglacial granular beds. *Geophys. Res. Lett*. **43**, L071579. (doi:10.1002/2016gl071579)
47. Zoet LK, Iverson NR. 2020 A slip law for glaciers on deformable beds. *Science* **368**, 76–78. (doi:10.1126/science.aaz1183)
48. Hansen DD, Zoet LK. 2022 Characterizing sediment flux of deforming glacier beds. *J. Geophys. Res. Earth Surf* **127**, e2021JF006544. (doi:10.1029/2021JF006544)
49. Lliboutry L. 1968 General theory of subglacial cavitation and sliding of temperate glaciers. *J. Glaciol*. **7**, 21–58. (doi:10.3189/s0022143000020396)
50. Iken A. 1981 The effect of the subglacial water pressure on the sliding velocity of a glacier in an idealized numerical model. *J. Glaciol*. **27**, 407–421. (doi:10.1017/S0022143000011448)
51. Iken A, Röthlisberger H, Flotron A, Haeberli W. 1983 The uplift of unteraargletscher at the beginning of the melt season—a consequence of water storage at the bed? *J. Glaciol*. **29**, 28–47. (doi:10.3189/S0022143000005128)
52. Schoof C. 2005 The effect of cavitation on glacier sliding. Proc. R. Soc. A Math. Phys. Eng. Sci. **461**, 609–627. (doi:10.1098/rspa.2004.1350)
53. Gagliardini O, Cohen D, Råback P, Zwinger T. 2007 Finite-element modeling of subglacial cavities and related friction law. *J. Geophys. Res. Earth Surf* **112**, 1–11. (doi:10.1029/2006JF000576)
54. Bindschadler R. 1983 The importance of pressurized subglacial water in separation and sliding at the glacier bed. *J. Glaciol*. **29**, 3–19. (doi:10.3189/s0022143000005104)
55. Iken A, Bindschadler RA. 1986 Combined measurements of subglacial water pressure and surface velocity of Findelengletscher, Switzerland: conclusions about drainage system and sliding mechanism. *J. Glaciol*. **32**, 101–119. (doi:10.3189/s0022143000006936)
56. Holschuh N, Christianson K, Dienstfrey W, Hills B, Hoffman AO, Paden J, Winter K, Zuraw R. 2026 Entrained debris records regrowth of the Greenland Ice Sheet after the last interglacial. *Nat. Geosci* (doi:10.1038/s41561-026-01950-1)
57. Franke S, Wolovick M, Drews R, Jansen D, Matsuoka K, Bons PD. 2024 Sediment freeze-on and transport near the onset of a fast-flowing glacier in East Antarctica. *Geophys. Res. Lett*. **51**, e2023GL107164. (doi:10.1029/2023GL107164)
58. Mutter EL, Holschuh N. 2025 Advancing interpretation of incoherent scattering in ice penetrating radar data used for ice core site selection. *Cryosphere* **19**, 3159–3176. (doi:10.5194/egusphere-2024-2450)
59. Lilien DA *et al*. 2021 Brief communication: new radar constraints support presence of ice older than 1.5 Myr at Little Dome C. *Cryosphere* **15**, 1881–1888. (doi:10.5194/tc-15-1881-2021)
60. Ariho G, Paden JD, Hoffman A, Christianson KA, Holschuh N. 2022 Joint estimation of ice sheet vertical velocity and englacial layer geometry from multipass synthetic aperture radar data. In *IEEE Phased Array Systems & Technology*, Waltham, MA, USA. Piscataway, NJ: IEEE. (doi:10.1109/PAST49659.2022.9974985)
61. Open Polar Radar. 2024 opr (Version 3.0.1) [Computer software]. (doi:10.5281/zenodo.5683959). See https://gitlab.com/openpolarradar/opr/.
62. Holschuh N. 2025 Replication Data for: 'Radar Swath Imaging of Glaciers and Ice Sheets' Harvard Dataverse, V1 (doi:10.7910/DVN/F6IUX4)